BAU Journal - Science and Technology

Volume 2 | Issue 1
ISSN: 2706-784X

Article 6

December 2020

PHOTOLUMINESCENCE SPECTROSCOPIC STUDIES OF MN2O3/CO3O4-GLUCOSE/LACTOSE COMPLEXES

Alaa Abdallah
MS student, Faculty of Science, Beirut Arab University, Beirut, Lebanon, a.mabdallah@bau.edu.lb

Jamalat Al Boukhari
PhD student, Faculty of Science, Beirut Arab University, Beirut, Lebanon, j.boukhari@bau.edu.lb

Rana Najjar
Department of Chemistry, Faculty of Science, Beirut Arab University, Beirut, Lebanon, r.najjar@bau.edu.lb

PHOTOLUMINESCENCE SPECTROSCOPIC STUDIES OF MN2O3/ CO3O4-GLUCOSE/LACTOSE COMPLEXES

Abstract

As nanoparticles serve as mediators in the electron transfer between biomolecules and a biosensor's electrode surface, this study is dedicated to investigating Mn2O3 and Co3O4 nanoparticles and their photoluminescence effect that play a critical role in sensing glucose and lactose. The chemical coprecipitation method was adopted for preparing the nanoparticles that were characterized by X-Ray Diffraction, Transmission Electron Microscope, Fourier Transform Infrared spectroscopy, Energy Dispersive X-ray, UV-vis spectroscopy, and Vibrating Sample Magnetometry. It was found that the obtained Mn2O3 and Co3O4 nanoparticles were successfully prepared, with a crystallite size of 65.91 and 58.00 nm, respectively. The high specific surface area of 1.2808´104 and 0.5711´104 m2/kg was noticed for the Mn2O3 and Co3O4 nanoparticles that exhibited highly agglomerated cubic and spherical nanoparticles, respectively. The energy gap, Urbach energy, and steepness parameter were obtained (1.72 eV, 1.049 eV and 24.644´10-3 for Mn2O3 and 1.285/2.165 eV, 2.893 eV and 8.936´10-3 for Co3O4) and discussed. Antiferromagnetism and weak ferromagnetism were detected for Mn2O3 and Co3O4 nanoparticles, respectively, with higher saturation magnetization for Mn2O3 (2.435 emu/g). Moreover, the non-enzymatic glucose and lactose biosensor's compatibility was evaluated utilizing photoluminescence changes. The glucose/lactose interactions with Mn2O3 /Co3O4 nanoparticles were measured by photoluminescence spectroscopy, at room temperature, in a phosphate buffer medium. The addition of Mn2O3 nanoparticles to glucose and lactose demonstrated higher shifts in the photoluminescence intensities with larger binding constants (1625 and 1840 M-1) and more negative Gibbs energy (-17.608 and -18.753 kJ.mol-1). These characteristics promote the investigation of Mn2O3 nanoparticles in glucose and lactose biosensors.

Keywords

Mn2O3 /Co3O4 nanoparticles, coprecipitation, non-enzymatic, photoluminescence

1. INTRODUCTION

Metal oxide nanomaterials have increasingly interfered in almost all technologies. This is believed to be due to the novel properties of materials when diminished to the nanoscale and assembled in unique morphologies (Abdolmohammad-Zadeh et al., 2020). Among the various metal oxides, Mn_2O_3 and Co_3O_4 nanoparticles have attracted research interests that thrived into preparing them via various techniques and widely using them in several applications, including wastewater treatment photocatalytic applications, microwave absorption, supercapacitors, sensors, MRI, biomedicine, antibacterial, antioxidant and enzyme inhibition activity (Can et al., 2020; Deka et al., 2020; Jiang et al., 2020b; Khalil et al., 2020; Kubra et al., 2020; Letsholathebe et al., 2020; P. Liu et al., 2020; Shaheen & Ahmad, 2020; X. Wei et al., 2020; Xie et al., 2020; Yang et al., 2020; C. Zhang et al., 2020).

Nanomaterials have proven their profound influence in the sector of enzyme-free biosensors. The distinguishable properties of materials at the nanoscale regime, especially biocompatibility and high activity, miniaturized the bio-sensing devices along with enhancing their detection sensitivity and specificity (Hou et al., 2018; X. Zhang et al., 2009). The Mn_2O_3 and Co_3O_4 nanoparticles belong to the metal oxides that are considered beneficial for the non-enzymatic glucose determination, utilized as electro-catalysts for glucose oxidation (Ahmad et al., 2020). Vukojevic et al. (Vukojević et al., 2018) prepared disposal glucose biosensors using MnO_2 nanoparticles on graphene nanoribbons. A synergetic effect of manganese dioxide decorated by graphene nanoribbons increased the characteristics of the electrode surface. Kumar et al. (Kumar et al., 2017) studied the electrochemical detection of p-nitrophenol using MnO nanoparticles of different sizes. MnO nanoparticles were found useful for sensing harmful chemicals and in various in vivo biological applications. Moreover, a recent study by Waqas et al. (Waqas et al., 2020) was conducted on Pd-Mn nanoalloy supported on reduced graphene oxide (rGO) for the construction of non-enzymatic electrochemical sensor for glucose or even for any other analyte. Enhanced electrochemical efficacy of Pd-Mn/rGO electrocatalyst was explained by abundant electrocatalytic active sites formed during the Pd-Mn alloying and the electron transport ability of rGO. On the other hand, Li et al. (S.-J. Li et al., 2014) studied the performance of CoO_x nanoparticles/graphene oxide modified electrodes in amperometric enzyme-free glucose biosensors. The developed biosensor showed a short response time (less than 5 s), high sensitivity of 79.3 $\mu AmM^{-1}\ cm^{-2}$, and good selectivity. Also, Zheng et al. (Zheng et al., 2014) studied the reduced graphene oxide and Co_3O_4 nanocomposites for non-enzymatic glucose sensors. Superior electrochemical activity towards the oxidation of glucose was noticed. After Kang et al. (Kang et al., 2019) offered a detailed study on the key role of L-lysine on the synthesis of highly porous Co_3O_4 nanoplates via the hydrothermal method, the performance of the prepared Co_3O_4 nanoplates towards non-enzymatic glucose sensing was investigated. The glucose sensors fabricated by the obtained porous Co_3O_4 nanoplates exhibited high performance represented by several factors, including fast response time (within 5 s) and good stability at low applied potential (0.38 V vs. Ag/AgCl).

Recently, research interest has increased in the field of nano-fluorescent biosensors due to their high sensitivity, simple, fast, low cost, and low background signals (Bhardwaj et al., 2017; Hou et al., 2018). Chen et al. (C. Chen et al., 2018) reported a study on glucose fluorescent biosensor, based on water-soluble and pH-responsive silicon nanodots. Glucose in human serum samples was detected with high sensitivity and selectivity. Billingsley et al. (Billingsley et al., 2010) designed fluorescent nanosensors based on ion-selective optodes capable of detecting small molecules.

Previously, we investigated NiO nanoparticles, prepared via coprecipitation method, and their interactions with both glucose and lactose (Abdallah et al., 2019). NiO nanoparticles were utilized for lactose non-enzymatic biosensors, as it was implied from the UV absorption and fluorescence spectroscopic studies. The interactions of lactose-NiO nanoparticles were found to be stronger than that of glucose-NiO ones. In the present work, we investigate Mn_2O_3 and Co_3O_4 nanoparticles, prepared by the chemical coprecipitation method. Then, we study the photoluminescence interactions between the Mn_2O_3/Co_3O_4- glucose/lactose complexes to recognize the interaction of each one of these nanoparticles with glucose and lactose.

A comparative study is implemented between the Mn_2O_3/Co_3O_4 nanoparticles of the present study and the NiO nanoparticles of the previous study with glucose and lactose to perceive the metal oxide that is better to be utilized in glucose and lactose non-enzymatic biosensors.

2. EXPERIMENTAL ROUTE

2.1 Nanoparticles' Preparation

The prepared metal oxide, Mn_2O_3 and Co_3O_4, nanoparticles were synthesized by the chemical coprecipitation method. Starting from the preparation of 1 M chloride solutions, the convenient stoichiometry of the salt chlorides ($MnCl_2.4H_2O$ and $CoCl_2.6H_2O$) was dispersed in distilled water. Thereafter, titration with 4 and 3 M Sodium Hydroxide NaOH, was carried out to the $MnCl_2$ and $CoCl_2$ solutions, respectively, to reach a basic medium of pH 13. This high pH induces more hydroxyl ions that ensure suitable nucleation and growth for the prepared samples (Palanisamy & Raichur, 2009). Then, the obtained hydroxide solutions (Mn $(OH)_2$ and Co $(OH)_2$) were heated at 343 K for 2 h and 333 K for 4 h, respectively. The heated solutions were set to cool down, and then they were filtered and washed thoroughly by distilled water to reach a neutral pH (i.e. pH=7). The resultant precipitates were dried at 373 K overnight, ground, and then calcined. Specifically, the Mn_2O_3 were calcined at 823 K for 6 h and the Co_3O_4 were calcined at 973 K for 4 h. Finally, the powders were ball milled, applying a 5:1 weight ratio of the balls to powders, for 20 min with a speed of 400 rpm.

2.2 Characterization Techniques

The structural properties of the prepared metal oxides (Mn_2O_3 and Co_3O_4) were investigated by X-Ray Diffraction (XRD) of Bruker D8 focus and Cu–K_α radiation source (λ = 1.54056 Å). The morphology of the prepared metal oxides was tested by Transmission Electron Microscope (TEM), JEM 100CX, having a resolution of 0.1 nm, operated at 80 kV. Moreover, Energy Dispersive X-ray (EDX), EDAX-ZAF, operating at 20 kV, and Fourier Transform Infrared (FTIR) spectroscopy, Nicolet iS5 FTIR spectrometer, were used to gain insights about the elemental composition and the vibrational modes present in the samples. The optical properties of the samples were studied by dissolving 0.01 g of the nanoparticles (Mn_2O_3 and Co_3O_4) in 50 mL of ethanol, followed by 5 min of sonication. The samples' absorbance, energy gap, Urbach energy, and steepness parameter were determined from the absorbance spectra of the prepared solutions, measured at room temperature by Ultraviolet-visible (UV-vis) spectroscopy, V-670. The Vibrating Sample Magnetometer (VSM), Lakeshore 7410, was utilized to explore the hysteresis loop of the prepared oxides, from which the remnant magnetization, coercivity, saturation magnetization, and squareness were evaluated.

2.3 Photoluminescence Investigations

The prepared metal oxides (Mn_2O_3 and Co_3O_4) were then mixed, in different concentrations, with 1×10^{-4} M of glucose and lactose to study the change in their photoluminescence activity. These interactions were held in a phosphate buffer medium of concentration 0.1 M and pH 6.5. The photoluminescence (PL) spectroscopy, FP-8300 spectrofluorometer accompanied by a Xenon (Xe) lamp, was used for this study with a 273 nm excitation wavelength.

3. RESULTS AND DISCUSSIONS

3.1 Structural Analysis

Error! Reference source not found. reveals the XRD patterns, with the corresponding (*hkl*) Miller indices, for (a) Mn_2O_3 and (b) Co_3O_4 nanoparticles. Both spectra are assigned to the cubic phase of the Mn_2O_3 and Co_3O_4 nanoparticles with no extra phases or impurities. Similar results were reported in the literature (Ahmed et al., 2020; Anuradha & Raji, 2019; Feng et al., 2020; Gajendiran et al., 2020; Iqbal et al., 2020; Jiang et al., 2020a; Z. Li et al., 2020; Mahani et al., 2020; Teli et al., 2020; G. Wei et al., 2019).

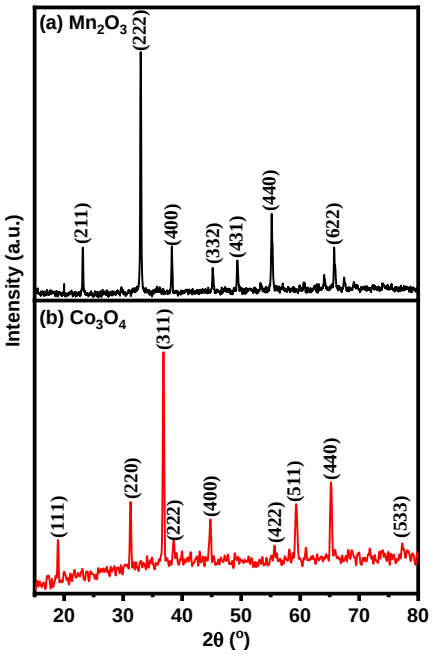

Fig.1: XRD patterns for (a) Mn_2O_3 and (b) Co_3O_4 nanoparticles

The lattice parameter (a) and the crystallite size (D) were obtained from Bragg's law (Eq. (1)) and Debye Scherrer's formula (Eq. (2)), respectively (Timoumi et al., 2020):

Eq. (1) $$a = d_{hkl}\sqrt{h^2 + k^2 + l^2}\,,$$

Eq. (2) $$D = \frac{k\lambda}{\beta \cos\theta}\,,$$

where, d_{hkl} is the interplanar distance between the adjacent planes, k = 0.9 is a shape factor, β is the full-width at half maximum, and θ is the glancing angle. The values of (a) and (D) are listed in Table 1. Moreover, the X-ray density (ρ_x) , the dislocation density (δ), and the specific surface area (*SSA*) were calculated and collected in Table 1, according to the following equations (Bharati et al., 2020; Jabbar et al., 2020):

Eq. (3) $$\rho_x = \frac{4M}{N_A a^3}\,,$$

Eq. (4) $$\delta = \frac{1}{D_{XRD}^2}\,,$$

Eq. (5) $$SSA = \frac{SA}{M} = \frac{SA}{\rho_x \times V}\,,$$

where, M is the molecular weight, N_A is Avogadro's number, SA is the surface area and V is the volume of the crystal. It is noticed that Mn_2O_3 has larger *SSA* than that of Co_3O_4 nanoparticles. Accordingly, since the catalytic activities are enhanced with larger *SSA* (Cui et al., 2019; Pedireddy et al., 2014), Mn_2O_3 may be more applicable than Co_3O_4 nanoparticles for non-enzymatic biosensors.

Table 1: The structural parameters of the Mn_2O_3 and Co_3O_4 nanoparticles

	Mn_2O_3	Co_3O_4
$a\,(Å)$	9.4169	8.091
$D\,(nm)$	65.910	58.000
$\rho_x \times 10^3\,(kg/m^3)$	1.256	3.019
$\delta \times 10^{14}\,(m^{-2})$	2.302	2.973
$SSA \times 10^4\,(m^2/kg)$	1.281	0.571
$D_p\,(nm)$	65.170	73.850
I	0.989	1.273

3.2 Morphological Analysis

The TEM images, shown in Error! Reference source not found. for the (a) Mn_2O_3 and (b) Co_3O_4 nanoparticles, depict highly agglomerated particles. The Mn_2O_3 nanoparticles exhibit a cubic nature, while the Co_3O_4 nanoparticles reveal spherical particles. The particle size distributions are drawn in Fig. 2 for (c) Mn_2O_3 and (d) Co_3O_4 nanoparticles, from which the average grain size (D_p) was computed and listed in Table 1.

Moreover, the crystallinity index (I), which is the ratio of the average grain size, computed from TEM images to the crystallite size, obtained from XRD patterns, is calculated and listed in Table 1 (Sahai & Goswami, 2014). It was found that both nanoparticles have crystallinity index values ~ 1, accounting for the monocrystalline nature of the prepared nanoparticles. Notice that the Co3O4 nanoparticles have a higher crystallinity index than Mn2O3, indicating the higher degree of agglomeration in Co3O4 nanoparticles (CNhopade et al., 2018). Such a crystallinity index can be explained by the agglomeration that most probably occurs during the preparation of the sample for the TEM measurements (Hafeez et al., 2020). Moreover, the agglomeration is ascribed to Ostwald's ripening process, where the formation of nanoparticles tends to reduce free energy (Voorhees, 1985). Thus, bigger and agglomerated nanoparticles are formed by the coalescence of smaller nanoparticles (Amiar Rodin et al., 2020).

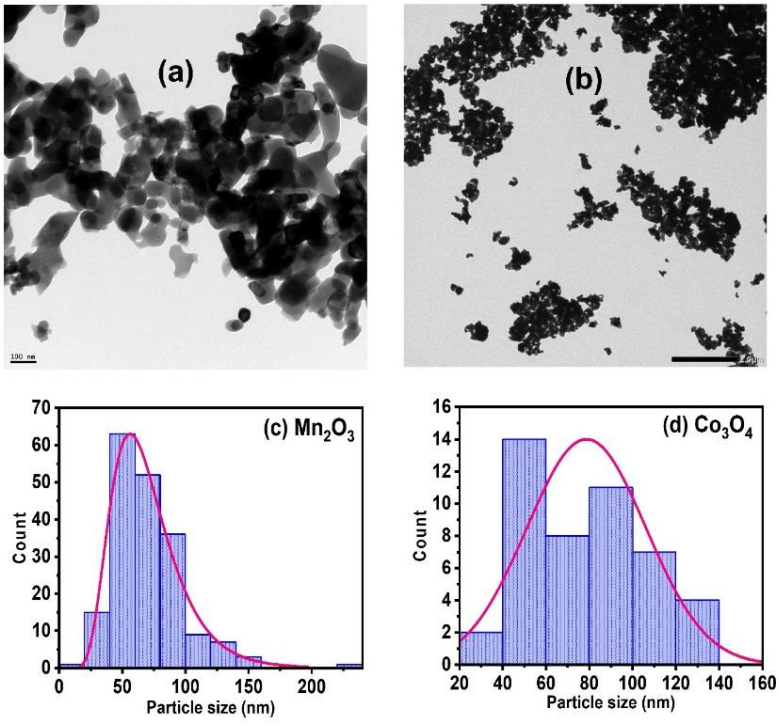

Fig.2: TEM images for (a) Mn_2O_3 and (b) Co_3O_4 nanoparticles with their particle size distribution histograms (c) and (d)

3.3 Vibrational bands and Elemental Composition

Error! Reference source not found. reveals the FTIR spectra of the investigated (a) Mn_2O_3 and (b) Co_3O_4 nanoparticles. In the group frequency region (region I) of both spectra, the presence of adsorbed water molecules and/or increased humidity is detected by the two peak ranges appearing at about 3440 cm^{-1} and 1645 cm^{-1}. Moreover, in the fingerprint region (region II), the two main peaks corresponding to the absorption bands of Mn_2O_3 and Co_3O_4 nanoparticles appear, identifying their successful formation. Specifically, the Mn_2O_3 spectrum establishes the two peaks at 610.36 and 530.33 cm^{-1}, ascribed to the stretching vibrations of Mn–O and Mn–O–Mn bonds, respectively. Besides, the peaks of the Co_3O_4 spectrum at 664 and 572 cm^{-1} are indicative of the stretching vibrational mode of Co^{2+}–O and Co^{3+}–O bonds, respectively. The same results were reported in the literature (H. Chen et al., 2020; Jassem et al., 2019; Medina et al., 2020; Son et al., 2019; Su et al., 2020).

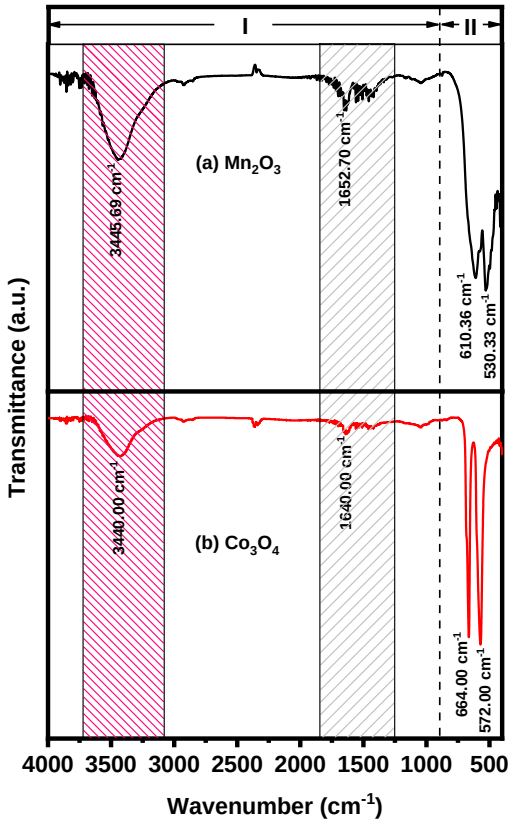

Fig.3: FTIR spectra for (a) Mn_2O_3 and (b) Co_3O_4 nanoparticles

The EDX graphs are represented in Error! Reference source not found. for (a) Mn2O3 and (b) Co3O4 nanoparticles with the corresponding elemental compositions listed in Table 2.

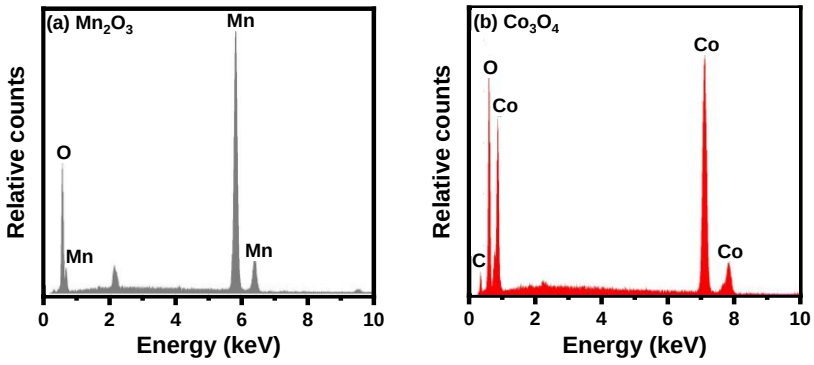

Fig.4: EDX spectra for (a) Mn_2O_3 and (b) Co_3O_4 nanoparticles

Apparent peaks of oxygen (O), manganese (Mn), and cobalt (Co) are observed, assuring the purity of the prepared samples. The carbon signal emerges from the mesh coating of the instrumental grid support (B. Liu et al., 2010).

Table 2: The elemental compositions of the Mn_2O_3 and Co_3O_4 nanoparticles

	Mn_2O_3		Co_3O_4		
	Mn	O	Co	O	C
Wt.%	80.44	19.56	60.96	30.42	8.63
At.%	54.50	45.50	28.31	52.04	19.66

3.4 Optical Analysis

The absorbance spectra for (a) Mn_2O_3 and (b) Co_3O_4 nanoparticles, investigated by UV-vis spectroscopy, are shown in Error! Reference source not found.. For Mn_2O_3 nanoparticles, two small peaks appear in the ultraviolet range (340 nm) and the visible range (553 nm), as clarified by the spectrum's fitting displayed in the inset of Fig. 5 (a). On the other hand, the absorbance spectrum of the Co_3O_4 nanoparticles shows two obvious peaks at 278 and 537 nm. These peaks are ascribed
to the charge transfer between the Co^{2+}–O^{2-} and Co^{3+}–O^{2-} ions localized at the tetrahedral and octahedral sites, respectively (Saravanakumar et al., 2018; Vennela et al., 2019).

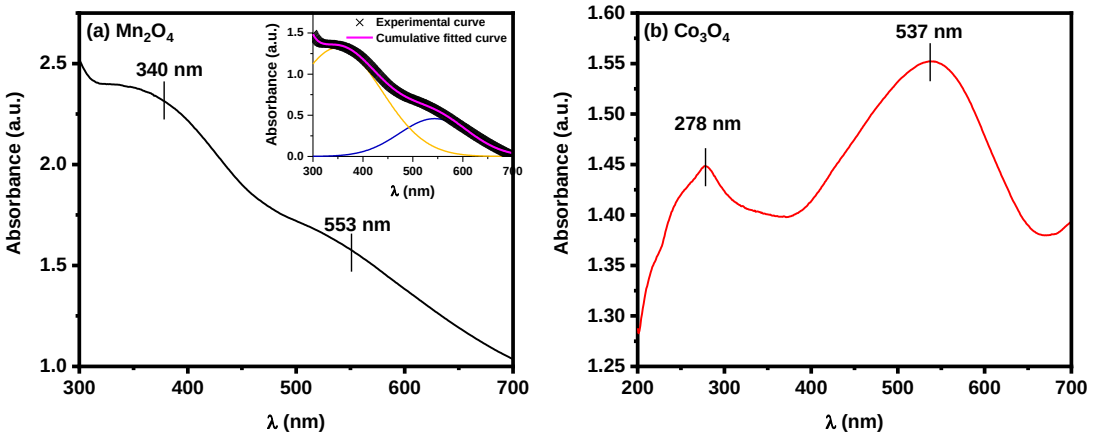

Fig.5: Absorbance spectra for (a) Mn_2O_3 and (b) Co_3O_4 nanoparticles

Moreover, Tauc plots, shown in Error! Reference source not found., were concerned to determine the energy gap (E_g) of the samples according to the following equation (Phan et al., 2019; Ravi Dhas et al., 2015):

Eq. (6) $$(\alpha h\nu)^{1/n} = \alpha_0 (h\nu - E_g),$$

where $\alpha = A/L$, A is the measured absorbance, L is the samples' thickness, n is an exponent related to the types of the transitions, α_0 is a material-dependent constant, and $h\upsilon$ is the energy. Accordingly, E_g was calculated for the direct allowed transitions (n=1/2) for both oxides and listed in Table 3. Mn_2O_3 nanoparticles have a small E_g, and Co_3O_4 has two energy gaps emerging from the two different charge transfer processes. However, the energy gap is highly affected by lattice distortions, non-stoichiometry, quantum confinement effect, and structural disorders.

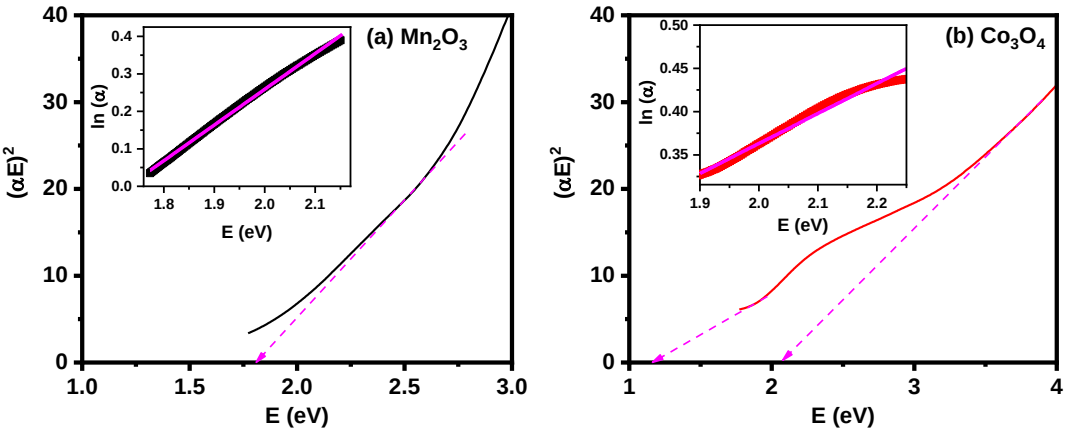

Fig.6: Tauc plot for (a) Mn_2O_3 and (b) Co_3O_4 nanoparticles

The Urbach energy (Eu) accounts for all possible defects, as it describes the width of the localized states in the bandgap (Turgut & Sönmez, 2014). Eu is computed from the slope of the logarithmic absorbance plot versus the energy, shown in the insets of Error! Reference source not found., according to the following equation (Kocyigit, 2018):

Eq. (7)
$$\log\alpha = \beta + \frac{h\nu}{E_u},$$

where β is a material-dependent factor. Also, the steepness parameter (σ), describes the harmonic interaction between the longitudinal optical phonons and excitons that describes the steepness of the exponential increase before the E_g. σ was discussed according to the following equation (Kocyigit, 2018; Turgut & Sönmez, 2014):

Eq. (8)
$$\sigma = \frac{k_B T}{E_u}.$$

The obtained values of E_u and σ are listed in Table 3. Co_3O_4 nanoparticles possess higher Urbach energy than Mn_2O_3 nanoparticles. This means that Co_3O_4 nanoparticles encounter more defects and disorders in their bonding that may arise due to the excitons and phonons of the multi-charges present in the structure (Ebrahimi et al., 2019).

Table 3: The optical parameters of the Mn_2O_3 and Co_3O_4 nanoparticles

	Mn_2O_3	Co_3O_4
$E_{g1}(eV)$	1.720	1.285
$E_{g2}(eV)$	-	2.165
$E_u(eV)$	1.049	2.893
$\sigma\times10^{-3}$	24.644	8.936

3.5 Magnetic Analysis

The room temperature hysteresis loops of the investigated (a) Mn_2O_3 and (b) Co_3O_4 are traced in Error! Reference source not found.. Mn_2O_3 exhibits an antiferromagnetic behavior; however, Co_3O_4 follows a weak ferromagnetic one. Similar results were reported in the literature (Anandha Babu et al., 2015; Pugazhvadivu et al., 2013; Zhu et al., 2008).

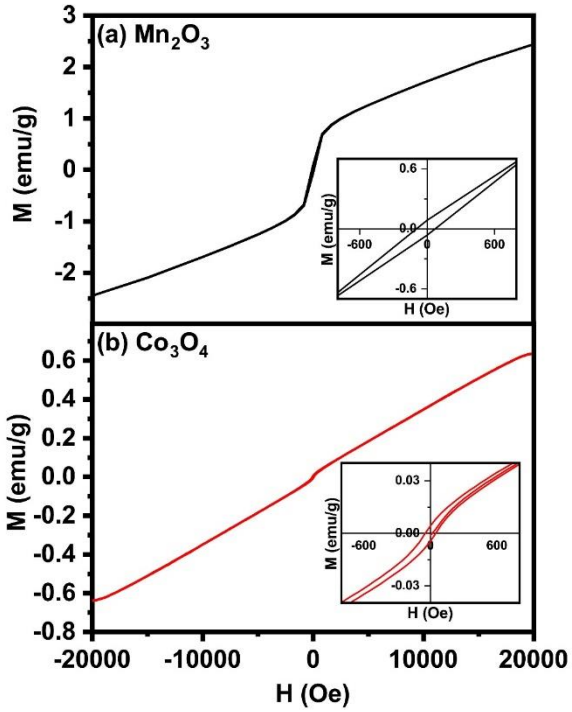

Fig.7: M-H loop for (a) Mn_2O_3 and (b) Co_3O_4 nanoparticles with corresponding insets at low field region

The remnant magnetization (M_r) and coercivity (H_c) were extracted from the loops and tabulated in Table 4. Furthermore, the saturation magnetization (M_s) was not reached even after applying a magnetic field of 20 kOe. Accordingly, the law of approach to saturation was implemented to determine the M_s, given by the following equation (Ghasemi et al., 2020; Singh et al., 2020):

Eq. (9)
$$M = M_S\left(1-\frac{a}{H}-\frac{b}{H^2}\right)+\chi H\,,$$

where M is the magnetization, H is the applied field, a is a constant related to structural defects and/or micro-stress, b is a constant related to anisotropy, and χ is the susceptibility at high field. However, below Curie temperature and high field limit, a/H and χH terms can be neglected (Selvaraj et al., 2020). Thus, equation (9) is reduced to:

Eq. (10)
$$M = M_S(1-\frac{b}{H^2}),$$

Therefore, the linear fit of M versus H^{-2}, shown in Error! Reference source not found., yields an intercept related to M_S values.

Table 4: The magnetic parameters of the Mn_2O_3 and Co_3O_4 nanoparticles

	Mn_2O_3	Co_3O_4
$M_r \times 10^{-3}\,(emu/g)$	73.597	4.370
$H_C\,(Oe)$	82.041	47.862
$M_S\,(emu/g)$	2.435	0.813
$S \times 10^{-3}$	30.225	5.375

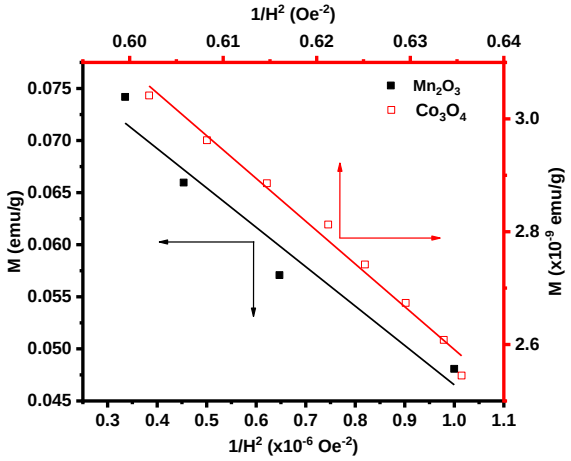

Fig.8: Magnetization versus $1/H^2$

The M_S values, listed in Table 4, signify that Mn_2O_3 has the highest value owing to the fact that the magnetic moment of manganese ($\sim 5\mu_B$) is higher than that of cobalt in tetrahedral site (Co^{2+} ($\sim 4.14\mu_B$), regardless of the diamagnetic Co^{3+} in the octahedral site (Moro et al., 2013; Pugazhvadivu et al., 2013). This makes Mn_2O_3 superior to Co_3O_4, since many biomedical applications require high M_S, as bacterial detection, protein purification, magnetic particle imaging (MPI), MRI contrast enhancement agents, biosensors, bio labeling, tracking of cells, hyperthermia, enzyme immobilization, and drug delivery (Amiri & Shokrollahi, 2013; Anbarasu et al., 2015; Elrefai et al., 2019; Huang & Juang, 2011). Hence, Mn_2O_3 has a greater potential than Co_3O_4 nanoparticles to be investigated in further applications. Moreover, the squareness (S) was estimated according to the following equation (Hessien et al., 2020; Shumskaya et al., 2020):

Eq. (11)
$$S = \frac{M_r}{M_S}.$$

The S-values are reported in Table 4, and it is noticed that Mn_2O_3 nanoparticles have larger value than Co_3O_4 nanoparticles due to its larger M_r. Also, the squareness values for both Mn_2O_3 and Co_3O_4 nanoparticles are less than 0.5, suggesting that the nanoparticles are related to multi-domain structure, following the Stoner-Wohlfarth model (Amiar Rodin et al., 2020).

3.6 Photoluminescence Analysis for Glucose and Lactose/ Nanoparticles Interactions

The photoluminescence spectra, shown in Error! Reference source not found., were measured at room temperature for different concentrations of Mn_2O_3 and Co_3O_4 nanoparticles (1×10^{-4} M – 10×10^{-4} M) with a constant concentration of glucose and lactose (1×10^{-4} M) dissolved in a phosphate buffer medium. Upon addition of Mn_2O_3 and Co_3O_4 nanoparticles to glucose and lactose in increased concentrations, the photoluminescence peak in the range of 300-302 nm increased by 34%, 6%, 42%, and 27% for Mn_2O_3 with glucose, Co_3O_4 with glucose, Mn_2O_3 with lactose and Co_3O_4 with lactose, respectively. These enhancements of intensities reveal the formation of oxides-carbohydrates complexes (Mn_2O_3-glucose, Co_3O_4-glucose, Mn_2O_3-lactose, and Co_3O_4-lactose) (Abo El-Maali et al., 2019). The photoluminescence enhancements may be originated from the charge delocalization and the increased rigidity of the oxides (Mn_2O_3 and Co_3O_4), by coordination to the carbohydrates (glucose and lactose) (Abo El-Maali et al., 2019; Ji et al., 2013). However, beyond the discussed range, the photoluminescence intensity for Mn_2O_3 with glucose has flipped, like that; the intensity was reduced upon the concentration addition of Mn_2O_3 nanoparticles.

Moreover, the photoluminescence intensity of Co_3O_4 with glucose, in 320-400 nm range, did not follow a normal trend; and the addition of Mn_2O_3 and Co_3O_4 nanoparticles to lactose revealed an independent-concentration behavior for the photoluminescence intensity. It can be surmised that the active photoluminescence region for the interactions of Mn_2O_3 and Co_3O_4 nanoparticles with glucose and lactose is in the range of 280-320 nm. Furthermore, the modified Stern-Volmer equation was applied to find quantitatively the binding constant (*K*) between the formed complexes (Cao & He, 1998):

Eq. (12)
$$\frac{1}{\Delta I} = \frac{1}{K\Delta I'[M]} + \frac{1}{\Delta I'},$$

where ΔI represents the change in the photoluminescence intensities between the added nanoparticles and the carbohydrates (glucose and lactose), $\Delta I'$ is a constant related to the formed complex, and [M] represents the different concentrations of the nanoparticles [Mn_2O_3] and [Co_3O_4]. Eq. (12) is represented by the double reciprocal plot of Fig. 10, from which K was found and its values are traced in Error! Reference source not found..

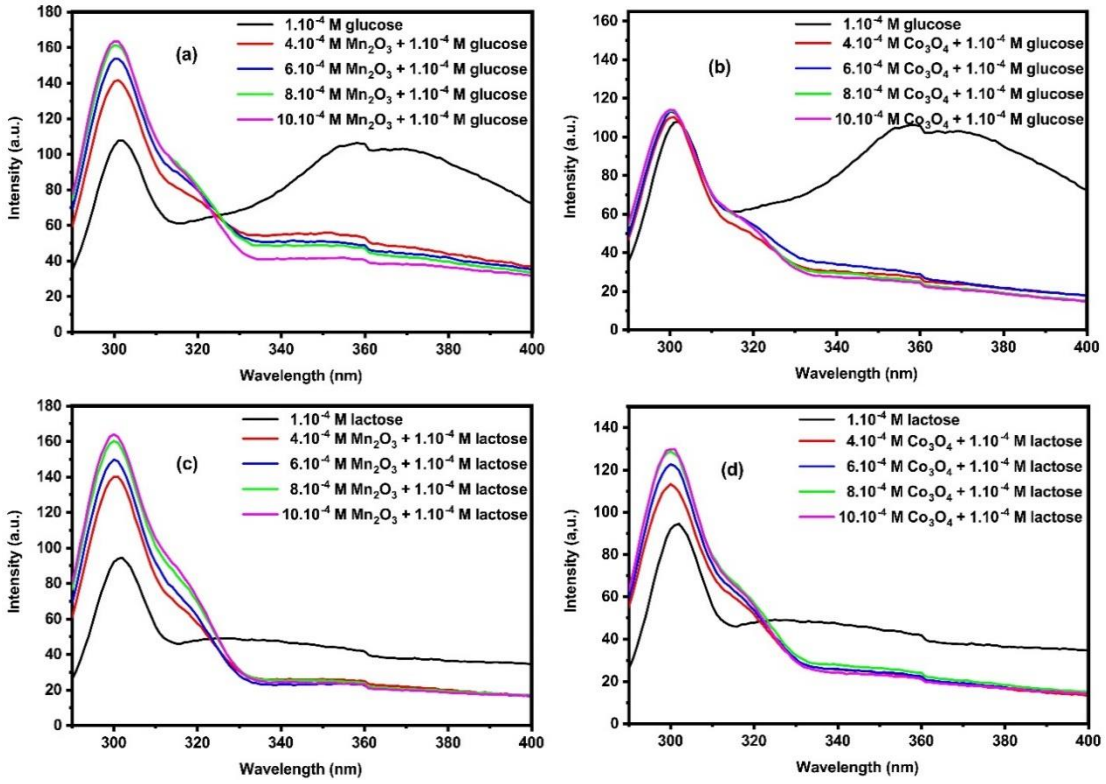

Fig.9: Photoluminescence for (a) glucose- Mn_2O_3 (b) glucose- Co_3O_4 (c) lactose- Mn_2O_3 and (d) lactose- Co_3O_4 complexes

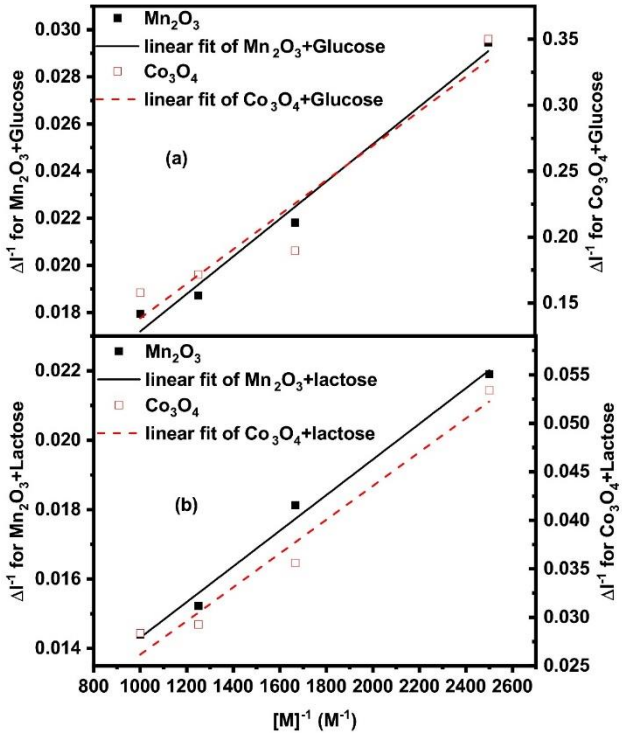

Fig.10: Double reciprocal plot (a) Mn_2O_3 and $Co_3O_4$with glucose and (b) Mn_2O_3 and $Co_3O_4$with lactose

The calculated values were compared to those obtained previously (Abdallah et al., 2019), where the interactions of NiO nanoparticles with both glucose and lactose were investigated. It is noted that the Mn_2O_3-lactose complex has the highest binding constant amongst the discussed oxides. To elucidate the type of these interactions, the Gibbs energy (ΔG^0) was calculated from the following thermodynamics equation (Paketurytė et al., 2019):

Eq. (13) $$\Delta G^0 = -2.303RT \log K ,$$

where R is the ideal gas constant. The calculated values are traced in Error! Reference source not found.. The interactions of the Mn_2O_3-lactose complex exhibited the smallest ΔG^0 among the three studied oxides (NiO, Mn_2O_3, and Co_3O_4) assuring that this complex has the most stable and spontaneous interactions (Mafuwe et al., 2019; Marques et al., 2019).

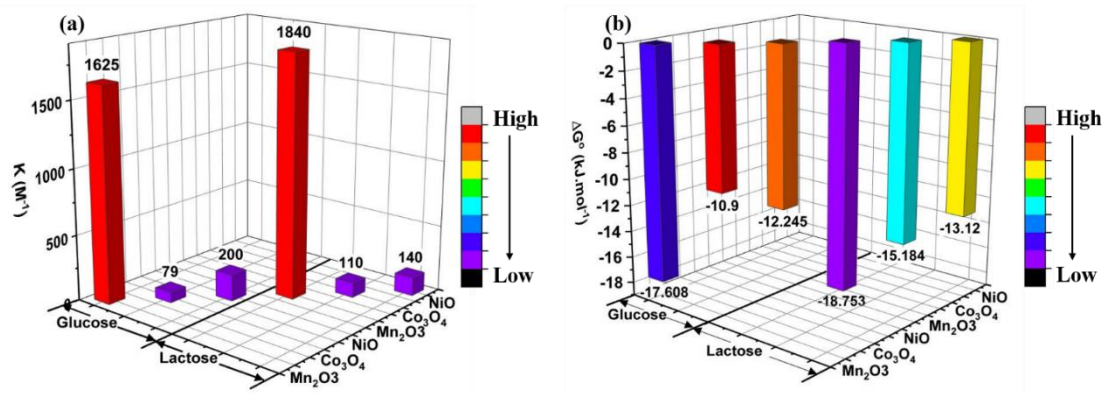

Fig.11: (a) the binding constant and (b) Gibb's energy of the formed complexes

4. CONCLUSIONS

As a conclusion, Mn_2O_3 and Co_3O_4 nanoparticles were successfully prepared by the chemical coprecipitation route. They exhibited a cubic crystal structure with a crystallite size of 65.91 and 58.00 nm for Mn_2O_3 and Co_3O_4 nanoparticles, respectively. Mn_2O_3 nanoparticles displayed a higher SSA due to the larger crystallite size and a smaller crystallinity index accounting for less agglomeration. Additionally, Mn_2O_3 nanoparticles acquired smaller Urbach energy, accounting for fewer defects in the sample. This confirmed the presence of less dislocation density in the Mn_2O_3 nanoparticles, following the XRD results. Besides, Mn_2O_3 nanoparticles showed a higher saturation magnetization and squareness-parameter arising from its antiferromagnetic nature, confronting the weak ferromagnetic nature of the Co_3O_4 nanoparticles. These characteristics contributed to higher binding constant, steadier, and spontaneous interactions with glucose and lactose. To sum up, Mn_2O_3 nanoparticles can be considered viable candidates for glucose and lactose non-enzymatic biosensors.

ACKNOWLEDGEMENT

This work was done at the Materials Science laboratory, Faculty of Science, Beirut Arab University.

REFERENCES

- Abdallah, A. M., Basma, H., & Awad, R. (2019). Preparation, Characterization, and Application of Nickel Oxide Nanoparticles in Glucose and Lactose Biosensors. *Modern Applied Science*, 13(6), 99. doi.org/10.5539/mas.v13n6p99
- Abdolmohammad-Zadeh, H., Ayazi, Z., & Hosseinzadeh, S. (2020). Application of Co_3O_4 nanoparticles as an efficient nano-sorbent for solid-phase extraction of zinc (II) ions. *Microchemical Journal*, 153, 104268. doi.org/10.1016/j.microc.2019.104268
- Abo El-Maali, N., Wahman, A. Y., Aly, A. A. M., Nassar, A. Y., & Sayed, D. M. (2019). Estimating of the binding constant of the anticancer 5-fluorouracil with Samarium and Europium. *Inorganic Chemistry Communications*, 107, 107440. doi.org/10.1016/j.inoche.2019.06.010
- Ahmad, R., Khan, M., Khan, M. R., Tripathy, N., Khan, M. I. R., Mishra, P., ... & Khosla, A. (2020). Nano-donuts shaped nickel oxide nanostructures for sensitive non-enzymatic electrochemical detection of glucose. *Microsystem Technologies*, 1-6.
- Ahmed, S., Lee, M.-C., Rim, H.-R., Lee, H.-K., Shim, J., & Park, G. (2020). Highly porous Co_3O_4 and Ni-deposited Co_3O_4 nanoflowers as bifunctional catalysts for oxygen reduction and evolution reactions. *Inorganic Chemistry Communications*, 113, 107799. doi.org/10.1016/j.inoche.2020.107799
- Amiar Rodin, N. L., Sahar, M. R., & Mohd-Noor, F. (2020). Magnetic analysis of cobalt oxide nanoparticles comprised boro-tellurite glass with erbium lanthanide. *Journal of Magnetism and Magnetic Materials*, 496, 165931. doi.org/10.1016/j.jmmm.2019.165931
- Amiri, S., & Shokrollahi, H. (2013). The role of cobalt ferrite magnetic nanoparticles in medical science. *Materials Science and Engineering: C*, 33(1), 1–8. doi.org/10.1016/j.msec.2012.09.003
- Anandha Babu, G., Ravi, G., Hayakawa, Y., & Kumaresavanji, M. (2015). Synthesis and calcinations effects on size analysis of Co_3O_4 nanospheres and their superparamagnetic behaviors. *Journal of Magnetism and Magnetic Materials*, 375, 184–193. doi.org/10.1016/j.jmmm.2014.09.062
- Anbarasu, M., Anandan, M., Chinnasamy, E., Gopinath, V., & Balamurugan, K. (2015). Synthesis and characterization of polyethylene glycol (PEG) coated Fe_3O_4 nanoparticles by chemical co-precipitation method for biomedical applications. *Spectrochimica Acta Part A: Molecular and Biomolecular Spectroscopy*, 135, 536–539. doi.org/10.1016/j.saa.2014.07.059
- Anuradha, C. T., & Raji, P. (2019). Synthesis, Characterization and Anti-Microbial Activity of Oxalate-Assisted CO_3O_4 Nanoparticles Derived from Homogeneous Co-Precipitation Method. *International Journal of Nanoscience*, 18(05), 1950002. doi.org/10.1142/S0219581X19500029
- Bharati, V. A., Somvanshi, S. B., Humbe, A. V., Murumkar, V. D., Sondur, V. V., & Jadhav, K. M. (2020). Influence of trivalent Al–Cr co-substitution on the structural, morphological and Mössbauer properties of nickel ferrite nanoparticles. *Journal of Alloys and Compounds*, 821, 153501. doi.org/10.1016/j.jallcom.2019.153501

- Bhardwaj, N., Bhardwaj, S. K., Nayak, M. K., Mehta, J., Kim, K.-H., & Deep, A. (2017). Fluorescent nanobiosensors for the targeted detection of foodborne bacteria. *TrAC Trends in Analytical Chemistry*, 97, 120–135. doi.org/10.1016/j.trac.2017.09.010
- Billingsley, K., Balaconis, M. K., Dubach, J. M., Zhang, N., Lim, E., Francis, K. P., & Clark, H. A. (2010). Fluorescent Nano-Optodes for Glucose Detection. *Analytical Chemistry*, 82(9), 3707–3713. doi.org/10.1021/ac100042e
- Can, K., Üzer, A., & Apak, R. (2020). A manganese oxide (MnO_x)-Based colorimetric nanosensor for indirect measurement of lipophilic and hydrophilic antioxidant capacity. *Analytical Methods*, 12(4), 448–455. doi.org/10.1039/C9AY02027F
- Cao, Y., & He, X. (1998). Studies of interaction between Safranine T and double helix DNA by spectral methods. *Spectrochimica Acta Part A: Molecular and Biomolecular Spectroscopy*, 54(6), 883–892. doi.org/10.1016/S1386-1425(97)00277-1
- Chen, C., Zhang, Y., Zhang, Z., He, R., & Chen, Y. (2018). Fluorescent Determination of Glucose Using Silicon Nanodots. *Analytical Letters*, 51(18), 2895–2905. doi.org/10.1080/00032719.2018.1456547
- Chen, H., Xue, C., Cui, D., Li, Y., Wang, Y., & Zhang, W. (2020). Triangular Prism Shaped Co_3O_4 as a high-performance Electrode Material for Supercapacitors. *Int. J. Electrochem. Sci*, 15, 966–976.
- Chopade, S. C., Kore, I. G., Patil, S. P., Jadhav, N. D., Srinidhi, C., & Desai, P. A. (2018). Lattice geometry controlled synthesis of Cu–Doped nickel oxide nanoparticles. *Ceramics International*, *44*(5), 5621-5628.
- Cui, T., Dong, J., Pan, X., Yu, T., Fu, Q., & Bao, X. (2019). Enhanced hydrogen evolution reaction over molybdenum carbide nanoparticles confined inside single-walled carbon nanotubes. *Journal of Energy Chemistry*, 28, 123–127. doi.org/10.1016/j.jechem.2018.03.006
- Deka, K., Guleria, A., Kumar, D., Biswas, J., Lodha, S., Kaushik, S. D., Dasgupta, S., & Deb, P. (2020). Exclusive T2 MRI contrast enhancement by mesoporous carbon framework encapsulated manganese oxide nanoparticles. *Current Applied Physics*, 20(1), 89–95. doi.org/10.1016/j.cap.2019.10.010
- Ebrahimi, S., Yarmand, B., & Naderi, N. (2019). Enhanced optoelectrical properties of Mn-doped ZnS films deposited by spray pyrolysis for ultraviolet detection applications. *Thin Solid Films*, 676, 31–41. https://doi.org/10.1016/j.tsf.2019.02.046
- Elrefai, A. L., Yoshida, T., & Enpuku, K. (2019). Magnetic parameters evaluation of magnetic nanoparticles for use in biomedical applications. *Journal of Magnetism and Magnetic Materials*, 474, 522–527. doi.org/10.1016/j.jmmm.2018.11.022
- Feng, L., Fan, G., Yuan, Z., Wang, S., Ren, M., Liu, B., Yang, W., & Luo, C. (2020). Microstructures and electrochemical properties of Co_3O_4 anodes coated by silane coupling agents. *Journal of Alloys and Compounds*, 816, 152623. doi.org/10.1016/j.jallcom.2019.152623
- Gajendiran, J., Sivakumar, N., Parthasaradhi Reddy, C., & Ramya, J. R. (2020). The effect of calcination's temperature on the structural, morphological, optical behaviour, hemocompatibility and antibacterial activity of nanocrystalline Co_3O_4 powders. *Ceramics International*, 46(4), 5469–5476. doi.org/10.1016/j.ceramint.2019.10.261
- Ghasemi, R., Echeverría, J., Pérez-Landazábal, J. I., Beato-Lopez, J. J., Naseri, M., & Gómez-Polo, C. (2020). Effect of Cu substitution on the magnetic and magnetic induction heating response of $CdFe_2O_4$ spinel ferrite. *Journal of Magnetism and Magnetic Materials*, 499, 166201. doi.org/10.1016/j.jmmm.2019.166201
- Hafeez, M., Shaheen, R., Akram, B., Haq, S., Mahsud, S., Ali, S., & Khan, R. T. (2020). Green synthesis of cobalt oxide nanoparticles for potential biological applications. *Materials Research Express*, *7*(2), 025019.
- Hessien, M. M., El-Bagoury, N., Mahmoud, M. H. H., Alsawat, M., Alanazi, A. K., & Rashad, M. M. (2020). Implementation of La^{3+} ion substituted M-type strontium hexaferrite powders for enhancement of magnetic properties. *Journal of Magnetism and Magnetic Materials*, 498, 166187. doi.org/10.1016/j.jmmm.2019.166187
- Hou, Y., Wang, J., Jin, J., & Shang, C. (2018). Research and Application of Nano-Fluorescent Materials based on DNA. *IOP Conference Series: Materials Science and Engineering*, 394, 022013. doi.org/10.1088/1757-899X/394/2/022013

- Huang, S. H., & Juang, R. S. (2011). Biochemical and biomedical applications of multifunctional magnetic nanoparticles: a review. *Journal of Nanoparticle Research*, *13*(10), 4411.
- Iqbal, S., Fakhar-e-Alam, M., Atif, M., Amin, N., Ali, A., Shafiq, M., Ismail, M., Hanif, A., & Farooq, W. A. (2020). Photodynamic therapy, facile synthesis, and effect of sintering temperature on the structure, morphology, optical properties, and anticancer activity of Co_3O_4 nanocrystalline materials in the $HepG_2$ cell line. *Journal of Photochemistry and Photobiology A: Chemistry*, 386, 112130. doi.org/10.1016/j.jphotochem.2019.112130
- Jabbar, R., Sabeeh, S. H., & Hameed, A. M. (2020). Structural, dielectric and magnetic properties of Mn^{+2} doped cobalt ferrite nanoparticles. *Journal of Magnetism and Magnetic Materials*, 494, 165726. doi.org/10.1016/j.jmmm.2019.165726
- Jassem, E. K., Majeed, A. M. A., & Umran, N. M. (2019). The Effect of Temperature on Structural and optical properties of Manganese Oxide Nanoparticles. *Journal of Physics: Conference Series*, 1279, 012004. doi.org/10.1088/1742-6596/1279/1/012004
- Ji, J., Zhang, Y., Fu, J.-D., Liu, Z.-L., & Wen, Y.-H. (2013). Three New Metal–Organic Polymers Based on Flexible 3-(4-(Carboxymethoxy) Phenyl) Propanoic Acid: Crystal Structures, Luminescent and Magnetic Properties. *Journal of Inorganic and Organometallic Polymers and Materials*, 23(6), 1347–1353. doi.org/10.1007/s10904-013-9934-6
- Jiang, X., Gray, P., Patel, M., Zheng, J., & Yin, J.-J. (2020b). Crossover between anti- and pro-oxidant activities of different manganese oxide nanoparticles and their biological implications. *Journal of Materials Chemistry* B, 8(6), 1191–1201. doi.org/10.1039/C9TB02524C
- Kang, M., Zhou, H., Zhao, N., & Lv, B. (2019). Porous Co3O4 nanoplates as an efficient electromaterial for non-enzymatic glucose sensing. *CrystEngComm*, 22(1), 35–43. https://doi.org/10.1039/C9CE01396B
- Khalil, A. T., Ovais, M., Ullah, I., Ali, M., Shinwari, Z. K., & Maaza, M. (2020). Physical properties, biological applications and biocompatibility studies on biosynthesized single phase cobalt oxide (Co_3O_4) nanoparticles via Sageretia thea (Osbeck.). *Arabian Journal of Chemistry*, 13(1), 606–619. doi.org/10.1016/j.arabjc.2017.07.004
- Kocyigit, A. (2018). Structural, optical and electrical characterization of Mn_3O_4 thin films via Au composite. *Materials Research Express*, 5(6), 066422. doi.org/10.1088/2053-1591/aacb0d
- Kubra, K. T., Sharif, R., Patil, B., Javaid, A., Shahzadi, S., Salman, A., Siddique, S., & Ali, G. (2020). Hydrothermal synthesis of neodymium oxide nanoparticles and its nanocomposites with manganese oxide as electrode materials for supercapacitor application. *Journal of Alloys and Compounds*, 815, 152104. doi.org/10.1016/j.jallcom.2019.152104
- Kumar, V., Singh, K., Panwar, S., & Mehta, S. K. (2017). Green synthesis of manganese oxide nanoparticles for the electrochemical sensing of p-nitrophenol. *International Nano Letters*, 7(2), 123–131. doi.org/10.1007/s40089-017-0205-3
- Letsholathebe, D., Thema, F. T., Mphale, K., Mohamed, H. E. A., Holonga, K. J., Ketlhwaafetse, R., & Chimidza, S. (2020). Optical and structural stability of Co_3O_4 nanoparticles for photocatalytic applications. *Materials Today: Proceedings*. doi.org/10.1016/j.matpr.2020.05.205
- Li, S. J., Du, J. M., Chen, J., Mao, N. N., Zhang, M. J., & Pang, H. (2014). Electrodeposition of cobalt oxide nanoparticles on reduced graphene oxide: a two-dimensional hybrid for enzyme-free glucose sensing. *Journal of Solid State Electrochemistry*, *18*(4), 1049-1056.
- Li, Z., Song, K., Wang, K., Chen, L., Wei, D., Lv, Y., Yu, Y., Yang, B., Yuan, L., & Hu, X. (2020). Fabrication of carbon cloth supporting MnO_x and its application in $Li–O_2$ batteries. *Nanotechnology*, 31(16), 165709. doi.org/10.1088/1361-6528/ab674f
- Liu, B., Zhang, X., Shioyama, H., Mukai, T., Sakai, T., & Xu, Q. (2010). Converting cobalt oxide subunits in cobalt metal-organic framework into agglomerated Co_3O_4 nanoparticles as an electrode material for lithium ion battery. *Journal of Power Sources*, 195(3), 857–861. doi.org/10.1016/j.jpowsour.2009.08.058
- Liu, P., Wang, Y., Han, L., Cai, Y., Ren, H., Ma, T., Li, X., Petrenko, V. A., & Liu, A. (2020). Colorimetric Assay of Bacterial Pathogens Based on Co_3O_4 Magnetic Nanozymes Conjugated with Specific Fusion Phage Proteins and Magnetophoretic Chromatography. *ACS Applied Materials & Interfaces*, 12(8), 9090–9097. doi.org/10.1021/acsami.9b23101
- Mafuwe, P. T., Moyo, M., Mugadza, T., Shumba, M., & Nyoni, S. (2019). Cobalt oxide nanoparticles anchored polyaniline-appended cobalt tetracarboxy phthalocyanine, modified glassy

carbon electrode for facile electrocatalysis of amitrole. *Journal of Solid State Electrochemistry*, 23(1), 285–294. doi.org/10.1007/s10008-018-4131-8

- Mahani, R. M., Darwish, A. G., & Ghoneim, A. M. (2020). Dielectric Relaxation Processes in Mn2O3/Reduced Graphene Oxide Nanocomposites. *Journal of Electronic Materials*. https://doi.org/10.1007/s11664-019-07913-0
- Marques, J. G. O., Costa, A. L., & Pereira, C. (2019). Gibbs free energy (ΔG) analysis for the NaOH (sodium-oxygen-hydrogen) thermochemical water splitting cycle. *International Journal of Hydrogen Energy*, 44(29), 14536–14549. doi.org/10.1016/j.ijhydene.2019.04.064
- Medina, M. S., Zenatti, A., & Escote, M. T. (2020). Fast Synthesis of Co_3O_4 by Microwave-Assisted Hydrothermal Treatment. *Journal of Nanomaterials*, 2020, 1–8. doi.org/10.1155/2020/2535019
- Moro, F., Yu Tang, S. V., Tuna, F., & Lester, E. (2013). Magnetic properties of cobalt oxide nanoparticles synthesised by a continuous hydrothermal method. *Journal of Magnetism and Magnetic Materials*, 348, 1–7. doi.org/10.1016/j.jmmm.2013.07.064
- Paketurytė, V., Linkuvienė, V., Krainer, G., Chen, W.-Y., & Matulis, D. (2019). Repeatability, precision, and accuracy of the enthalpies and Gibbs energies of a protein–ligand binding reaction measured by isothermal titration calorimetry. *European Biophysics Journal*, 48(2), 139–152. doi.org/10.1007/s00249-018-1341-z
- Palanisamy, P., & Raichur, A. M. (2009). Synthesis of spherical NiO nanoparticles through a novel biosurfactant mediated emulsion technique. *Materials Science and Engineering: C*, 29(1), 199–204. doi.org/10.1016/j.msec.2008.06.008
- Pedireddy, S., Lee, H. K., Tjiu, W. W., Phang, I. Y., Tan, H. R., Chua, S. Q., Troadec, C., & Ling, X. Y. (2014). One-step synthesis of zero-dimensional hollow nanoporous gold nanoparticles with enhanced methanol electrooxidation performance. *Nature Communications*, 5(1), 1–9. doi.org/10.1038/ncomms5947
- Phan, T. D., Vo, C. M., Tran, T. M. T., Luu, T. L. A., & Nguyen, X. S. (2019). Structural and bandgap properties of titanium dioxide nanotube/graphene oxide composites prepared by a facile hydrothermal method. *Materials Research Express*, 6(10), 105054. doi.org/10.1088/2053-1591/ab3a0b
- Pugazhvadivu, K. S., Ramachandran, K., & Tamilarasan, K. (2013). Synthesis and Characterization of Cobalt doped Manganese Oxide Nanoparticles by Chemical Route. *Physics Procedia*, 49, 205–216. doi.org/10.1016/j.phpro.2013.10.028
- Ravi Dhas, C., Venkatesh, R., Jothivenkatachalam, K., Nithya, A., Suji Benjamin, B., Moses Ezhil Raj, A., Jeyadheepan, K., & Sanjeeviraja, C. (2015). Visible light driven photocatalytic degradation of Rhodamine B and Direct Red using cobalt oxide nanoparticles. *Ceramics International*, 41(8), 9301–9313. doi.org/10.1016/j.ceramint.2015.03.238
- Sahai, A., & Goswami, N. (2014). Structural and vibrational properties of ZnO nanoparticles synthesized by the chemical precipitation method. *Physica E: Low-Dimensional Systems and Nanostructures*, 58, 130–137. doi.org/10.1016/j.physe.2013.12.009
- Saravanakumar, P., Muthukumar, M., Muthuchudarkodi, R. R., & Ramkumar, P. (2018). Piper Nigrum Mediated Green Synthesis, Charecterization of Undoped Cobalt Oxide and Cerium Ion Doped Cobalt Oxide Nanoparticles.
- Selvaraj, S., Gandhi, U., Mangalanathan, U., & Berchmans, L. J. (2020). Enhancement of Saturation Magnetization and Remanence of $BaFe_{12}O_{19}$ Materials Prepared by NaCl–KCl and Hexamine as Flux. *IEEE Magnetics Letters*, 11, 1–5. doi.org/10.1109/LMAG.2020.2965889
- Shaheen, I., & Ahmad, K. S. (2020). Synthesis of binary metal oxide-doped Co_3O_4 nanoparticles by organic template and investigation of its structural, optical and electrochemical properties. *Journal of Materials Science: Materials in Electronics*, 31(13), 10323–10333. doi.org/10.1007/s10854-020-03580-8
- Shumskaya, A., Bundyukova, V., Kozlovskiy, A., Zdorovets, M., Kadyrzhanov, K., Kalkabay, G., & Kaniukov, E. (2020). Evolution of morphology, structure, and magnetic parameters of Ni nanotubes with growth in pores of a PET template. *Journal of Magnetism and Magnetic Materials*, 497, 165913. doi.org/10.1016/j.jmmm.2019.165913
- Singh, A., Pathak, S., Kumar, P., Sharma, P., Rathi, A., Basheed, G. A., Maurya, K. K., & Pant, R. P. (2020). Tuning the magnetocrystalline anisotropy and spin dynamics in $Co_xZn_{1-x}Fe_2O_4$

($0 \leq x \leq 1$) nanoferrites. *Journal of Magnetism and Magnetic Materials*, 493, 165737. doi.org/10.1016/j.jmmm.2019.165737

- Son, Y.-H., Bui, P. T. M., Lee, H.-R., Akhtar, M. S., Shah, D. K., & Yang, O.-B. (2019). A Rapid Synthesis of Mesoporous Mn2O3 Nanoparticles for Supercapacitor Applications. *Coatings*, 9(10), 631. doi.org/10.3390/coatings9100631
- Su, L., Wang, L., Yao, X., Yin, X., Zhang, H., Zhao, M., Liu, S., Wang, Z., Wang, J., & Zhang, D. (2020). Small size nanoparticles—Co_3O_4 based lateral flow immunoassay biosensor for highly sensitive and rapid detection of furazolidone. *Talanta*, 211, 120729. doi.org/10.1016/j.talanta.2020.120729
- Teli, A. M., Beknalkar, S. A., Patil, D. S., Pawar, S. A., Dubal, D. P., Burute, V. Y., Dongale, T. D., Shin, J. C., & Patil, P. S. (2020). Effect of annealing temperature on charge storage kinetics of an electrospun deposited manganese oxide supercapacitor. *Applied Surface Science*, 511, 145466. doi.org/10.1016/j.apsusc.2020.145466
- Timoumi, A., Albetran, H. M., Alamri, H. R., Alamri, S. N., & Low, I. M. (2020). Impact of annealing temperature on structural, morphological and optical properties of GO-TiO_2 thin films prepared by spin coating technique. *Superlattices and Microstructures*, 139, 106423. doi.org/10.1016/j.spmi.2020.106423
- Turgut, G., & Sönmez, E. (2014). A Study of Pb-Doping Effect on Structural, Optical, and Morphological Properties of ZnO Thin Films Deposited by Sol–Gel Spin Coating. *Metallurgical and Materials Transactions A*, 45(8), 3675–3685. doi.org/10.1007/s11661-014-2281-6
- Vennela, A. B., Mangalaraj, D., Muthukumarasamy, N., Agilan, S., & Hemalatha, K. V. (2019). Structural and Optical Properties of Co_3O_4 Nanoparticles Prepared by Sol-gel Technique for Photocatalytic Application. *Int. J. Electrochem. Sci*, 14, 3535–3552. doi.org/10.20964/2019.04.40
- Voorhees, P. W. (1985). The theory of Ostwald ripening. *Journal of Statistical Physics*, 38(1), 231–252. doi.org/10.1007/BF01017860
- Vukojević, V., Djurdjić, S., Ognjanović, M., Fabián, M., Samphao, A., Kalcher, K., & Stanković, D. M. (2018). Enzymatic glucose biosensor based on manganese dioxide nanoparticles decorated on graphene nanoribbons. *Journal of Electroanalytical Chemistry*, 823, 610–616. doi.org/10.1016/j.jelechem.2018.07.013
- Waqas, M., Lan, J., Zhang, X., Fan, Y., Zhang, P., Liu, C., Jiang, Z., Wang, X., Zeng, J., & Chen, W. (2020). Fabrication of Non-enzymatic Electrochemical Glucose Sensor Based on Pd−Mn Alloy Nanoparticles Supported on Reduced Graphene Oxide. *Electroanalysis*, 32(6), 1226–1236. doi.org/10.1002/elan.201900705
- Wei, G., Zhou, Z., Zhao, X., & An, C. (2019). Template growth of ultrasmall Co_3O_4 nanoparticles: A highefficiency electrocatalyst for alkaline oxygen evolution reaction. *IOP Conference Series: Materials Science and Engineering*, 612, 022038. doi.org/10.1088/1757-899X/612/2/022038
- Wei, X., Chen, J., Ali, M. C., Munyemana, J. C., & Qiu, H. (2020). Cadmium cobaltite nanosheets synthesized in basic deep eutectic solvents with oxidase-like, peroxidase-like, and catalase-like activities and application in the colorimetric assay of glucose. *Microchimica Acta*, 187(6), 314. doi.org/10.1007/s00604-020-04298-4
- Xie, X., Ni, C., Lin, Z., Wu, D., Sun, X., Zhang, Y., Wang, B., & Du, W. (2020). Phase and morphology evolution of high dielectric CoO/Co_3O_4 particles with Co_3O_4 nanoneedles on surface for excellent microwave absorption application. *Chemical Engineering Journal*, 396, 125205. doi.org/10.1016/j.cej.2020.125205
- Yang, J., Xu, X., Zhou, X., Jiang, S., Chen, W., Shi, S., Wang, D., & Liu, Z. (2020). Ultrasmall Co_3O_4 Nanoparticles Confined in P, N-Doped Carbon Matrices for High-Performance Supercapacitors. *The Journal of Physical Chemistry C*, 124(17), 9225–9232. doi.org/10.1021/acs.jpcc.0c01539
- Zhang, C., Peng, Y., Song, Y., Li, J., Yin, F., & Yuan, Y. (2020). Periodic Three-Dimensional Nitrogen-Doped Mesoporous Carbon Spheres Embedded with Co/Co3O4 Nanoparticles toward Microwave Absorption. *ACS Applied Materials & Interfaces*, 12(21), 24102–24111. doi.org/10.1021/acsami.0c03105
- Zhang, X., Guo, Q., & Cui, D. (2009). Recent Advances in Nanotechnology Applied to Biosensors. *Sensors (Basel, Switzerland)*, 9(2), 1033–1053. doi.org/10.3390/s90201033

- Zheng, Y., Li, P., Li, H., & Chen, S. (2014). Controllable growth of cobalt oxide nanoparticles on reduced graphene oxide and its application for highly sensitive glucose sensor. *Int. J. Electrochem. Sci*, 9, 7369–7381.
- Zhu, H. T., Luo, J., Liang, J. K., Rao, G. H., Li, J. B., Zhang, J. Y., & Du, Z. M. (2008). Synthesis and magnetic properties of antiferromagnetic Co_3O_4 nanoparticles. *Physica B: Condensed Matter*, 403(18), 3141–3145. doi.org/10.1016/j.physb.2008.03.024